Stepped-Impedance Common-Mode Filter for Differential Lines Enhanced With Resonant Planes

Arif Ege Engin, *Member, IEEE*, Nisarg Modi, and Hiroyasu Oomori

***Abstract*—High-speed digital systems require differential lines for chip-to-chip links. A common concern in differential lines is the presence of common-mode noise, which is a major contributor to signal integrity problems in high-speed digital systems. Common-mode noise is typically excited by skew. It can occur due to timing mismatches at the driver, length mismatches due to routing constraints, or phase velocity mismatches due to inhomogeneous dielectrics with fiber-weave effect. Common-mode noise results in increased crosstalk and electromagnetic interference on packages and boards. This paper presents a methodology based on varying the common-mode impedance of a differential line, while keeping the differential-mode constant. The variation in impedance results in a filter response solely for the common-mode signals, improving the noise immunity of the differential pair. This design is applied on stripline-type differential lines and the performance is enhanced by adjusting the ground via pitch to create resonant planes with a high-impedance current return path for common-mode signals.**

***Index Terms*—Common-mode filter, differential lines, electromagnetic bandgap filter, mixed-mode scattering parameters.**

I. Introduction

DIFFERENTIAL signaling has been used in designing high-speed package and board interconnects because of its high immunity to noise, crosstalk, and electromagnetic interference. However, unintended common-mode signals couple to the transmission lines and degrade the signal and power integrity of the high-speed channel in practice. Therefore, the common-mode noise suppression at high frequencies in differential lines is of the highest interest.

There are several approaches proposed for the common-mode noise suppression in differential lines. The high permeability common-mode choke is the conventional way to suppress the common-mode noise, but it is effective only for a megahertz frequency range [1]. The common-mode noise suppression by varying the cross section of the transmission lines has been proposed in [2]. A periodically patterned ground plane is used in [3] to achieve interruption of common-mode return currents. A similar approach in [4] is also based on a patterned ground plane, but supports return currents by coplanar ground strips. The basic principle is the periodical variation of the common-mode impedance that results in a filter response for the common-mode signals. This is also used in [5], where the reference plane is changed to a different layer periodically to alter the common-mode impedance.

We have recently introduced the stepped-impedance common-mode filter in [6]. This filter is applicable at higher gigahertz frequencies while not requiring a change in the cross section of the transmission lines. It is based on varying the common-mode impedance of a differential line while keeping the differential-mode impedance constant. This variation in impedance results in a filter response solely for the common-mode signals, improving the noise immunity of the differential pair. In [7], we have enhanced the performance of this common-mode filter by introducing the resonant-plane common-mode filter. This new filter makes use of the ground via pitch as an additional variable. An additional resonance is introduced in the reference plane at the desired frequency, complementing the previous stepped-impedance common-mode filter performance by creating a dual-mode filtering response. Alternatively, a higher attenuation on a larger stopband of frequencies by combining these two resonances can also be achieved. In this paper, we extend our initial work by providing an extensive study of this common-mode filter including simulation to hardware correlations on a test board.

II. Stepped-Impedance Common-Mode Filter

A. Design Equations

In this section, we present a unified view of stepped-impedance common-mode filters. Such filters are also referred to as electromagnetic bandgap common-mode filters, as they depend on a periodic variation of the even-mode impedance while keeping the odd-mode impedance constant [4], [5], [8]. We present a simple closed-form design equation to determine the stopband of such filters and propose a new stripline implementation. Afterwards, we present that a second stopband response is achievable by adjusting the ground via locations.

As an example, an ideal differential line is simulated with a differential impedance of $Z\text{diff} = 100\ \Omega$, which corresponds to an odd-mode impedance of $Zo = 50\ \Omega$. The stepped-impedance common-mode filter is realized by alternating the even-mode impedance between $Ze^l = 50\ \Omega$ and $Ze^h = 100\ \Omega$ as shown in Fig. 1. This results in a filter response for the common-mode signal, whereas the differential signal is unaffected. The stopband of the filter is symmetrically centered around 10 GHz,

Manuscript received May 10, 2018; revised June 20, 2018; accepted July 14, 2018. *(Corresponding author: Arif Ege Engin.)*

A. E. Engin and N. Modi are with the Department of Electrical and Computer Engineering, San Diego State University, San Diego, CA 92182 USA (e-mail: aengin@mail.sdsu.edu; n4nisarg@gmail.com).

H. Oomori is with Sumitomo Electric Industries, Yokohama 244-8588, Japan (e-mail: oomori-hiroyasu@sei.co.jp).

Color versions of one or more of the figures in this paper are available online at http://ieeexplore.ieee.org.

Digital Object Identifier 10.1109/TEMC.2018.2862636

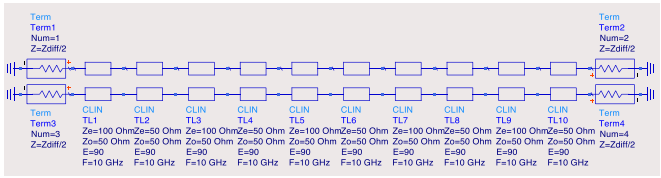

(a)

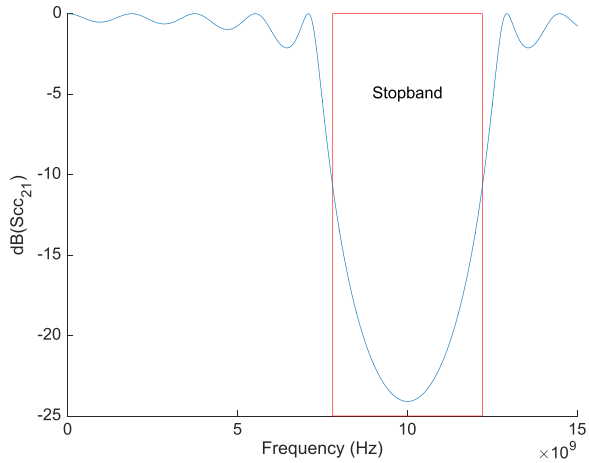

(b)

Fig. 1. (a) Stepped-impedance common-mode filter for a differential line. (b) Common-mode signal is effectively filtered around the design frequency of 10 GHz.

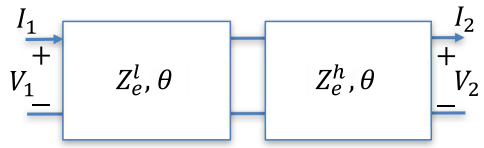

Fig. 2. Unit cell of a periodic structure consisting of transmission lines with equal electrical length but different characteristic impedances.

where each differential-line section is quarter wavelength. The cutoff frequency of the stepped-impedance common-mode filter depends on the difference between Ze^l and Ze^h.

To determine the stopband, the stepped-impedance filter will be considered as an infinitely periodic structure of alternating impedances and equal electrical lengths. A unit cell of such a structure for solely the common-mode signals can then be considered as shown in Fig. 2. The ABCD parameters of this structure can be calculated from the product of the *ABCD* parameters of each section as

$$\begin{bmatrix} A & B \\ C & D \end{bmatrix} = \begin{bmatrix} \cos\theta & jZ_e^l \sin\theta \\ \frac{j\sin\theta}{Z_e^l} & \cos\theta \end{bmatrix} \begin{bmatrix} \cos\theta & jZ_e^h \sin\theta \\ \frac{j\sin\theta}{Z_e^h} & \cos\theta \end{bmatrix}$$

$$= \begin{bmatrix} \cos^2\theta - \sin^2\theta \frac{Z_e^l}{Z_e^h} & j\cos\theta\sin\theta\,(Z_e^l + Z_e^h) \\ j\cos\theta\sin\theta(\frac{1}{Z_e^l} + \frac{1}{Z_e^h}) & \cos^2\theta - \sin^2\theta \frac{Z_e^h}{Z_e^l} \end{bmatrix}. \quad (1)$$

The boundaries of the stopbands and passbands of such an infinitely periodic structure can be calculated following [9] by finding the electrical lengths of structures where

$$\frac{A+D}{2} = \pm 1. \quad (2)$$

Substituting (1) into (2) yields

$$\cos^2\theta - \frac{\sin^2\theta}{2}\left(\frac{Z_e^l}{Z_e^h} + \frac{Z_e^h}{Z_e^l}\right) = \pm 1. \quad (3)$$

The choice of a positive sign for the right-hand side gives the trivial result of $\theta = 0$. Using the negative sign for the right-hand side yields

$$\sin^2\theta = \frac{4Z_e^l Z_e^h}{\left(Z_e^h + Z_e^l\right)^2}. \quad (4)$$

A simpler formula is obtained in terms of the cosine function as

$$\cos\theta = \pm\frac{Z_e^h - Z_e^l}{Z_e^h + Z_e^l}. \quad (5)$$

The on-set and off-set frequencies of the first stopband occur accordingly at the following electrical lengths:

$$\theta_l = \cos^{-1}\left(\frac{Z_e^h - Z_e^l}{Z_e^h + Z_e^l}\right) \quad (6)$$

$$\theta_h = \pi - \cos^{-1}\left(\frac{Z_e^h - Z_e^l}{Z_e^h + Z_e^l}\right). \quad (7)$$

This equation is a simpler version of the closed-form equations given in [5]. Applying this to the example shown in Fig. 1 yields

$$f_l = \cos^{-1}\left(\frac{1}{3}\right) \times \frac{2}{\pi} \times 10^{10} = 7.8 \times 10^9 \quad (8)$$

$$f_h = \left[\pi - \cos^{-1}\left(\frac{1}{3}\right)\right] \times \frac{2}{\pi} \times 10^{10} = 12.2 \times 10^9 \quad (9)$$

which match well with the simulation results as shown in the figure.

B. Stripline Implementation of a Stepped-Impedance Common-Mode Filter

Two specific implementations of the stepped-impedance common-mode filter are given in [4] and [5] for microstrip lines. In this paper, we present an alternative design for striplines.

The design in [5] varies the common-mode impedance by changing the reference plane on a multilayer board. The disadvantages of this approach are the requirement of additional layers and vias to stitch the reference planes together. The design in [4] does not increase the layer count, however, the requirement of coplanar waveguide ground strips limits the routing density of multiple differential line channels together. The new stripline design in this paper does not increase the layer count, and requires no additional vias.

The basic stripline configuration for edge-coupled differential lines is shown in Fig. 3(a). The top plane is removed for every other quarter-wavelength section, resulting in embedded microstrip configuration as shown in Fig. 3(b). The even-mode

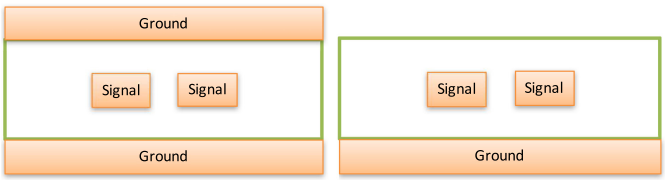

Fig. 3. (a) Edge-coupled differential striplines. (b) Removing the top plane results in embedded microstrip lines with a higher even-mode impedance.

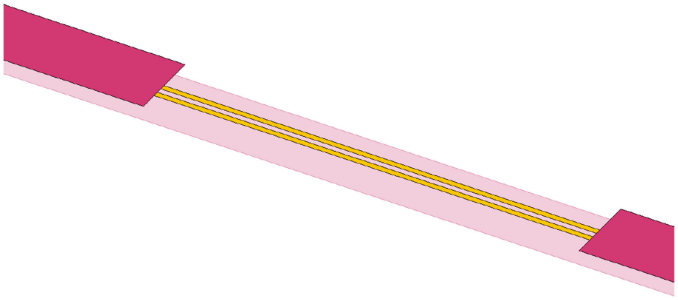

Fig. 4. Embedded microstrip section between two differential stripline sections.

impedance is significantly higher for the embedded microstrip sections, because of the removal of the top plane. The odd-mode impedance mostly depends on the geometries of the signal lines, and hence, does not change significantly. Therefore, a common-mode filter will be created by alternating stripline sections with embedded-microstrip sections for the differential line.

As a numerical example, a differential stripline embedded in FR-4 with a dielectric constant of 4 and loss tangent of 0.02 is considered. For the sake of simplicity, the copper thickness is neglected. The top and bottom dielectrics are each 5-mil thick, resulting in a 50-Ω odd-mode impedance for a width and spacing of 4 mils. The center frequency of the stopband is chosen as 5 GHz, which results in a quarter-wavelength of approximately 300 mils in the dielectric medium. Three unit cells are used, resulting in a total length of 1800 mils for the whole structure. Fig. 4 shows the three-dimensional view of an embedded microstrip section between two stripline sections.

The even-mode impedance changes from $Ze^l = 62\,\Omega$ for the stripline sections to $Ze^h = 88\,\Omega$ for the embedded microstrip sections, calculated using the controlled-impedance line designer in Keysight ADS [10]. As a result, the on-set and off-set frequencies of the stopband can be calculated as

$$f_l = \cos^{-1}(0.17) \times \frac{2}{\pi} \times 10^{10} = 4.5 \times 10^9 \tag{10}$$

$$f_h = \left[\pi - \cos^{-1}(0.17)\right] \times \frac{2}{\pi} \times 10^{10} = 5.6 \times 10^9. \tag{11}$$

Fig. 5 demonstrates the effectiveness of the stepped-impedance common-mode filter compared to a baseline that is purely a stripline configuration. This simulation was done using the full-wave simulator Sonnet [11]. The stopband around 5 GHz is observed in Scc21 parameters of the common-mode filter. The attenuation at the stopband can be increased by using

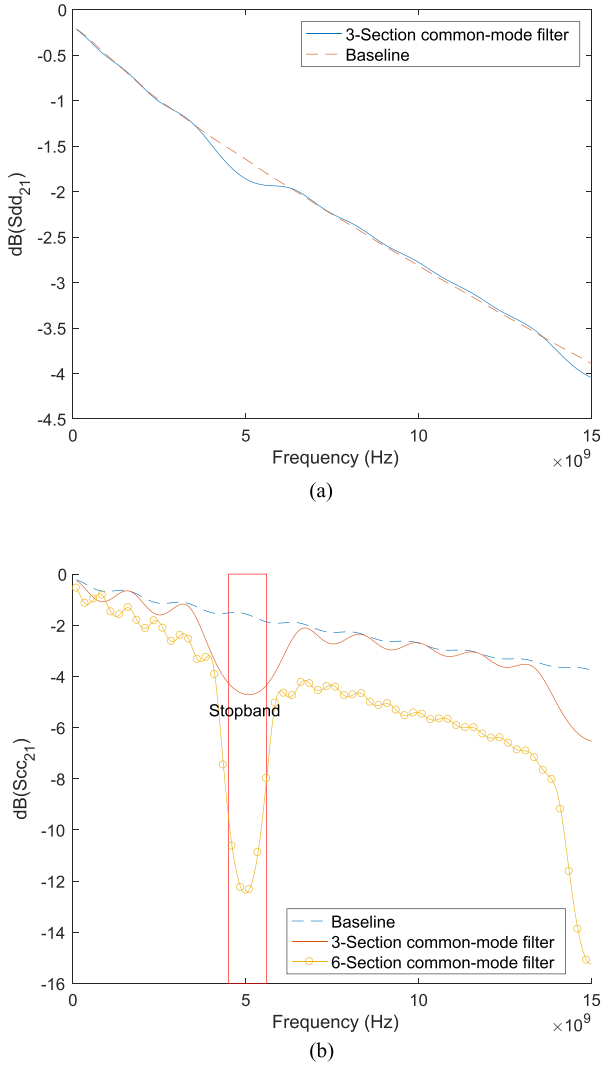

Fig. 5. Differential line with width and spacing of 4 mils. (a) Insertion loss for the differential-mode signals is not deteriorated by the filter except for a slight deviation around 5 GHz. (b) Common-mode signals are effectively filtered around the design frequency of 5 GHz. Filter attenuation is increased by using more unit cells in the design.

more sections in the filter. A longer filter was simulated by doubling the length of the filter using six unit cells. Fig. 5(b) shows the improvement in attenuation for the longer filter. Outside of the stopband, the insertion loss is also more for the longer filter, due to the increased dielectric and conductor losses.

A slight deviation in Sdd21 from the baseline case can be observed around 5 GHz. This is primarily due to the small change in the odd-mode characteristic impedance from 50 Ω in the stripline to 55 Ω in the embedded microstrip line. If the lines are more tightly coupled, this variation should even be smaller. As an example, a second case was simulated where a tighter coupling was achieved by choosing the width as 3 mils and spacing as 2 mils. This resulted in odd-mode impedances of 49 Ω and 51 Ω for the stripline and embedded microstrip sections. Fig. 6 shows that there is no significant change in Sdd21, whereas a similar stopband is obtained for Scc21. The same filter was also simulated using multilayered transmission

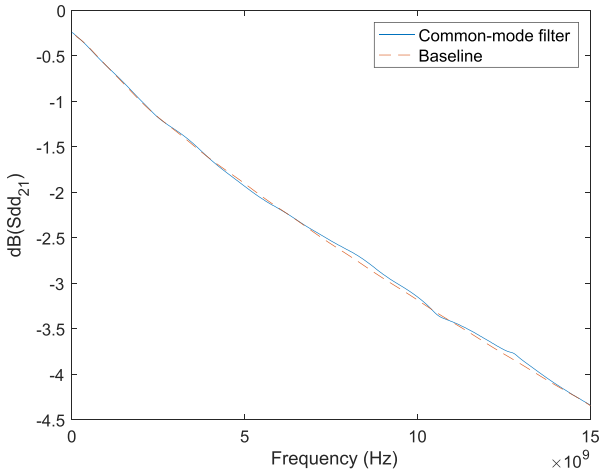

(a)

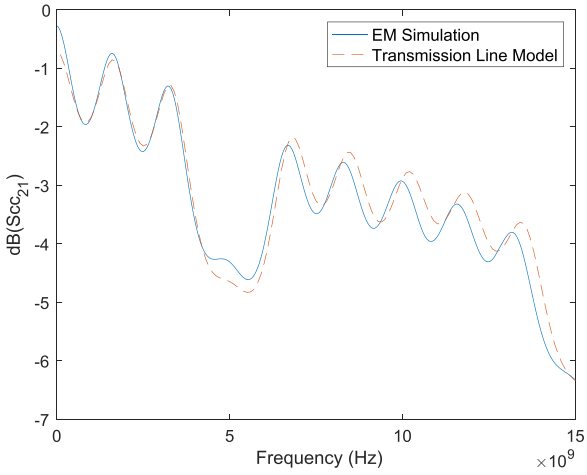

(b)

Fig. 6. Differential line with width of 3 mils and spacing of 2 mils is tighter coupled compared the example in Fig. 5. (a) Insertion loss for the differential-mode signals has no significant deviation. (b) Circuit simulation using transmission line models in ADS matches electromagnetic simulation in Sonnet.

line models in ADS and shows good agreement with Sonnet. In circuit simulation, a small copper thickness of 0.1 mil was used to be able to incorporate the conductor losses.

III. Resonant-Plane Enhancement

The ground-via pitch for striplines as shown in Fig. 7 is not a critical parameter for ideal lines, as long as the port excitations are purely in the stripline mode. The stepped-impedance filter, on the other hand, restricts the return current to the bottom ground plane at the embedded microstrip segments; therefore, the parallel-plate mode gets excited as well [12]. This provides an opportunity to use the ground via pitch as an additional variable to design the common-mode filter.

As an example, a common-mode filter was studied with a quarter-wavelength resonance of 26 GHz in the longitudinal direction. Here, we have used FR4 epoxy with $\varepsilon_r = 3.6$,

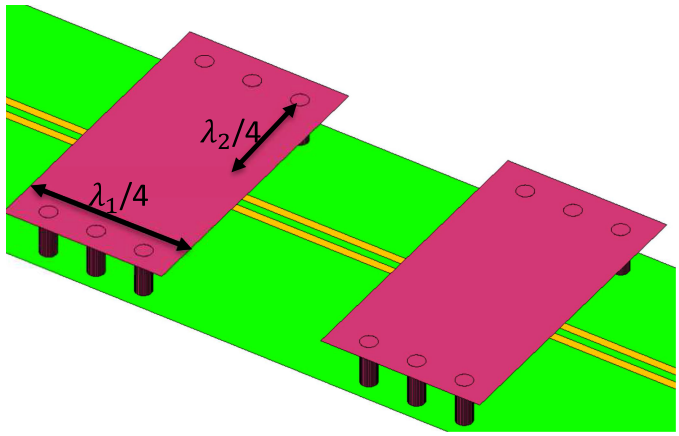

Fig. 7. Adjusting the ground via pitch ($\lambda_2/4$) results in an additional notch in the common-mode filter due to the lateral resonance.

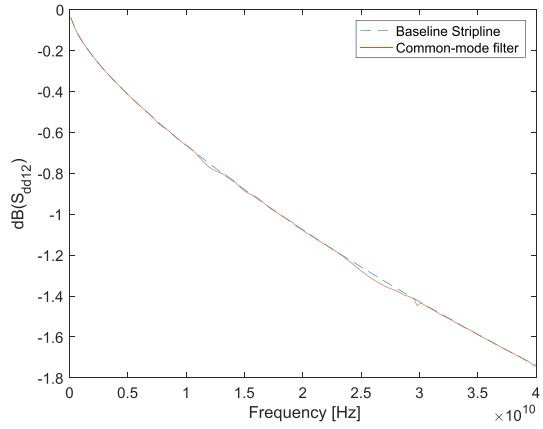

(a)

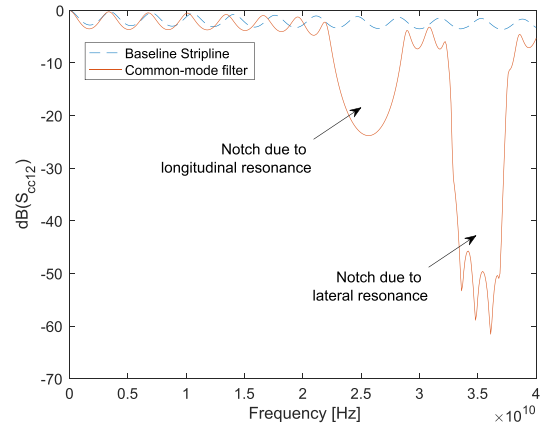

(b)

Fig. 8. (a) Insertion loss for the differential-mode signals is not deteriorated by the filter. (b) Common-mode filter has two notches that can be adjusted independently. Lateral resonance results in a stronger attenuation.

$\tan\delta = 0.007$, and thickness of 600 μm as the substrate material and assigned width and spacing of 75 μm and thickness of 18 μm to the differential traces, with each transmission-line section as 1500-μm long (total length of traces = 22 500 μm) to achieve the resonance in the longitudinal direction.

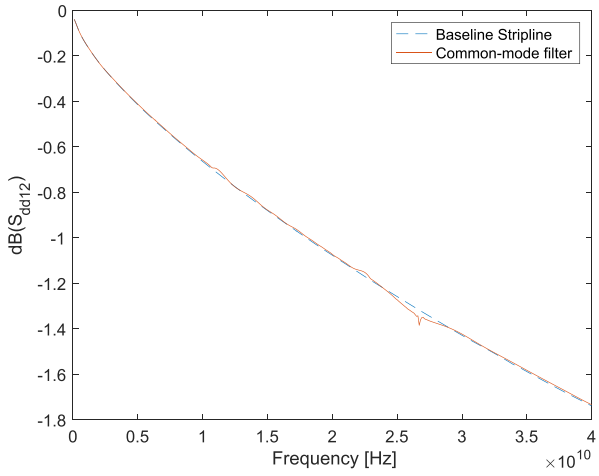

(a)

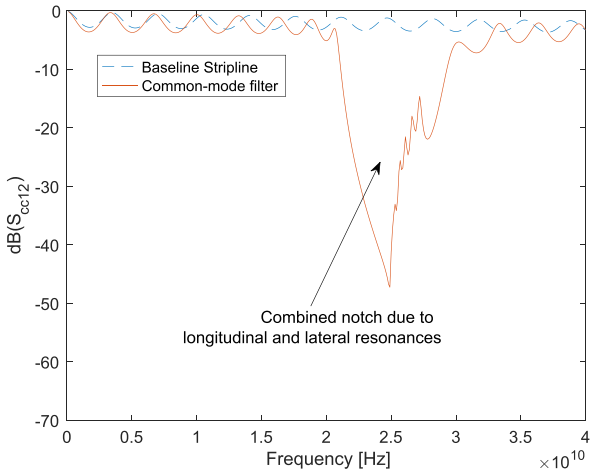

(b)

Fig. 9. Simulations after increasing the ground via pitch to 3300 μm. (a) Insertion loss for the differential-mode signals is not deteriorated by the filter. (b) Two notches are combined to obtain a wider stopband for common-mode signals.

The filter starts and ends with an embedded microstrip segment and has a ground width of 2500 μm. Considering that top ground patches have lengths of 1500 μm, a quarter-wavelength resonance of 34 GHz in the lateral direction is calculated using the microstrip model in ADS LineCalc. Sdd12 and Scc12 parameters have been extracted using HFSS [13]. In HFSS, we have assigned the radiation boundary at the top of the structure. The side boundaries are perfect electric boundaries representing the ground vias, whereas the metal layers are copper.

Comparison with the baseline case of the differential striplines shows that the filter does not affect the differential-mode insertion loss in Fig. 8. The resonant-plane common-mode filter design results in a new lateral resonance. The locations of the two stopbands are accurately estimated by the longitudinal and lateral resonances at 26 and 34 GHz based on the quarter-wavelength dimensions in Fig. 7.

In Fig. 9, we achieved a larger single stopband for the common-mode filter by increasing the width of the ground plane to 3300 μm so that the two resonances got combined. The differential-mode insertion loss (Sdd12) is maintained at a similar level. This example illustrates the use of the ground via pitch as an additional variable to obtain a large stopband for common-mode signals.

The design of this enhanced filter considering ground via locations can be efficiently done using dispersion diagrams for periodic structures. To generate the dispersion diagram, a single

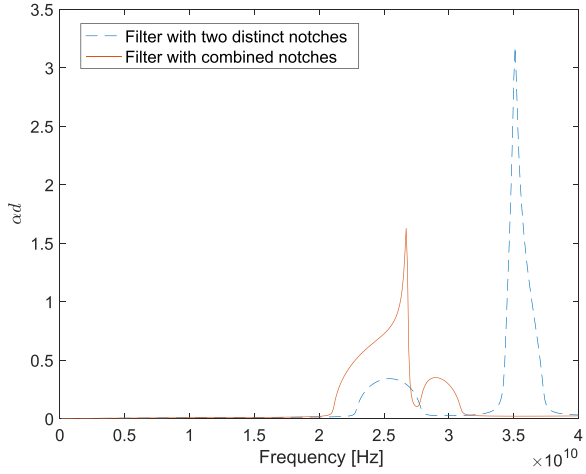

Fig. 10. Attenuation coefficient based on dispersion diagram analysis of a single unit cell confirms the stopbands of the filters in Fig. 8 ($\lambda_1 \neq \lambda_2$), and Fig. 9 ($\lambda_1 = \lambda_2$).

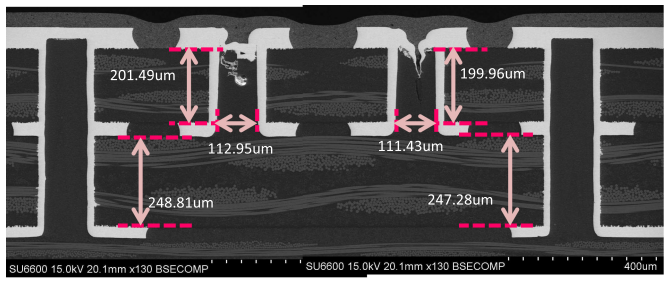

(a)

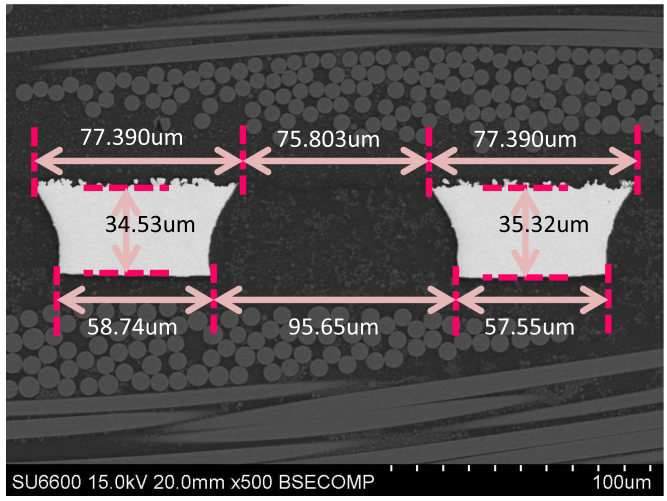

(b)

Fig. 11. Cross sections taken with a focused ion beam. Measurement of (a) dielectric thicknesses; and (b) width and spacing including the etching effect.

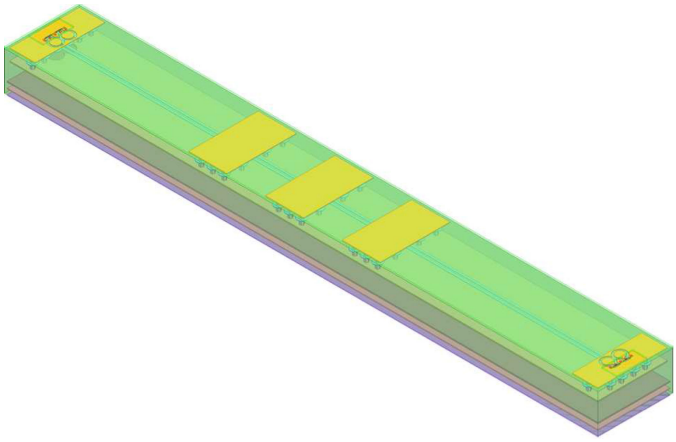

(a)

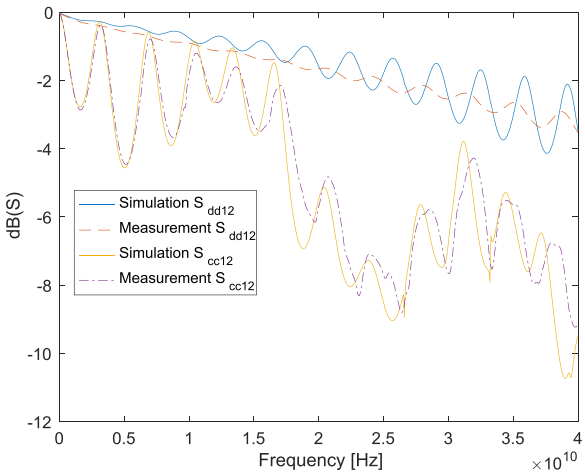

(b)

Fig. 12. (a) Common-mode filter using three sections. (b) Common mode effectively filtered around the center frequency of 26.5625 GHz.

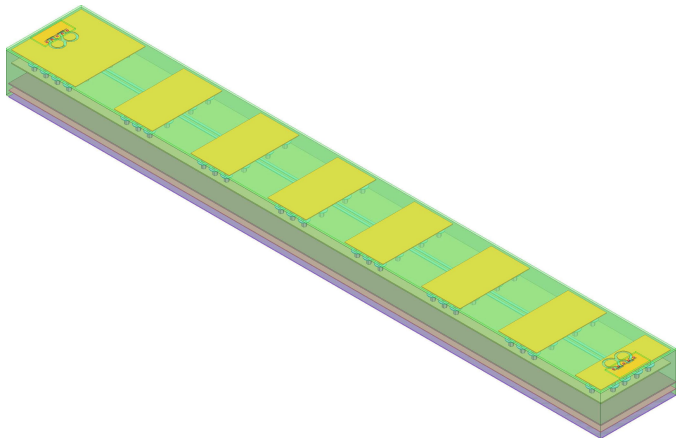

(a)

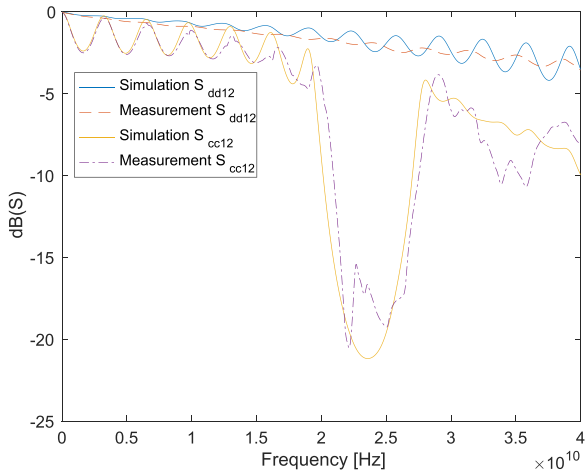

(b)

Fig. 13. (a) Common-mode filter using seven sections. (b) Common-mode isolation level improves for this seven-section filter as compared to the three-section filter of Fig. 12.

unit cell can be simulated, consisting of a cascaded half embedded microstrip segment, a full stripline segment, and another half embedded microstrip segment. This simulation setup defines the ports clearly on the embedded microstrip segments, so as to avoid shorting the stripline ground planes at a wave or box-wall port. From this simulation, the common-mode scattering parameters are obtained and converted to ABCD parameters. The dispersion characteristic can then be obtained from the ABCD parameters [9], [14] using

$$\cosh(\alpha d + j\beta d) = \frac{A + D}{2}. \tag{12}$$

Fig. 10 shows the attenuation coefficient obtained through dispersion diagram analysis for the examples in Figs. 8 and 9. The locations of the stopbands in the dispersion diagram match the ones observed in the common-mode insertion loss. The lateral resonance (as a function of λ_2 in Fig. 7) provided a larger attenuation compared to the longitudinal resonance (λ_1) in this example. The dispersion diagram analysis requires simulation of a single unit cell only; allowing efficient design and optimization of the common-mode filter.

IV. Measurement Results

A test board was fabricated to verify the performance of the common-mode filter. For accurate simulation comparison, cross sections were taken with a focused ion beam as shown in Fig. 11. The measured dielectric thicknesses and line width and spacing were then used in HFSS. The etching effect was included in the simulation geometry by using trapezoidal transmission lines.

HFSS simulations were carried out and compared against measurements for several test cases. The total length of the differential line was 21 mm for all cases and the common-mode filter was designed with a center frequency of 26.5625 GHz. This particular frequency is chosen to provide a common-mode filter solution for the practical case of a 400-Gb/s optical transceiver operating at 53.125 Gb/s per lane. Fig. 12 shows the performance of the common-mode filter using only three sections. Good simulation to measurement correlation is observed.

The common-mode filter performance in Fig. 12 can be improved in two possible ways. One option is to use more sections in the filter as shown in Fig. 13. Common-mode isolation level

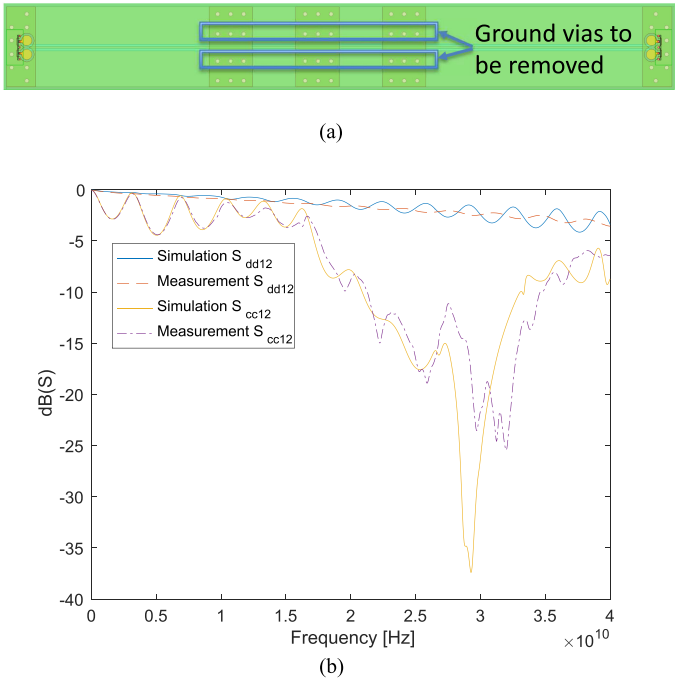

Fig. 14. (a) Closest vias to the stripline sections have been removed to introduce lateral resonance enhancing the performance of the common-mode filter. (b) Common-mode filter has a larger bandwidth and isolation compared to the original filter in Fig. 12.

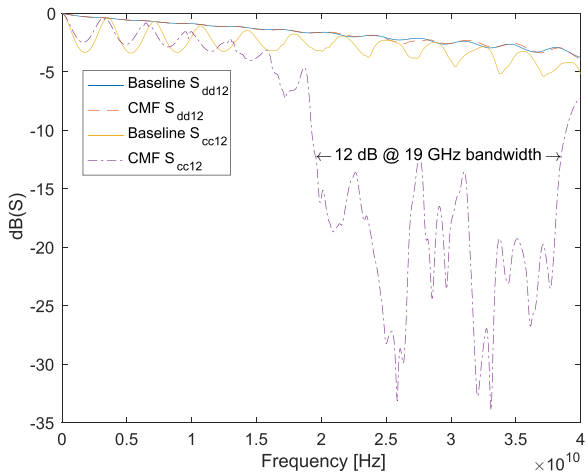

Fig. 15. Measured common-mode filter (CMF) performance including seven sections and with larger ground via pitch. The differential insertion loss is not affected compared to a baseline embedded microstrip differential line. Close to an octave of filter bandwidth is observed at an isolation level of 12 dB for the common-mode insertion loss.

improves for this seven-section filter as compared to the three-section filter of Fig. 12.

Another option for improvement would be introducing the lateral resonance by adjusting the ground via pitch. For this purpose, the closest vias to the stripline sections have been removed as shown in Fig. 14. This results in an additional notch in the filter performance in the vicinity of the center frequency of the filter. As expected, this enhanced common-mode filter has larger bandwidth and isolation compared to the original filter in Fig. 12.

As a final test case, both improvements were applied simultaneously by using seven sections and enhancing the filter performance by adjusting the ground via pitch. Fig. 15 shows a comparison of this common-mode filter with the baseline case, which is just a straight embedded microstrip differential line without any filter. The differential insertion loss is not affected as shown in the figure. Close to an octave of filter bandwidth is observed for an isolation level of 12 dB.

V. Conclusion

A simple design equation was introduced to estimate the on-set and off-set frequencies of stepped-impedance common-mode filters in differential lines. The filter is based on varying the common-mode impedance of a differential line, while keeping the differential-mode constant. A new implementation of this filter has been introduced for edge-coupled striplines. Full-wave simulations demonstrate that the common-mode signal is effectively filtered at the design frequency, whereas the differential-mode signal is not deteriorated. A resonant-plane enhancement is introduced to filter common-mode signals at an additional center frequency, which can be adjusted by the ground via pitch. The two frequencies can be combined to have increased attenuation over a larger stopband. A test board including common-mode filters was designed at a center frequency of 26.5625 GHz. The measurements showed good agreement with simulation in terms of mixed-mode scattering parameters. It was observed that the performance of this new-common mode filter is significantly improved by adjusting the ground via pitch, without affecting the differential insertion loss.

References

[1] K. Yanagisawa, F. Zhang, T. Sato, K. Yamasawa, and Y. Miura, "A new wideband common-mode noise filter consisting of Mn-Zn ferrite core and copper/polyimide tape wound coil," *IEEE Trans. Magn.*, vol. 41, no. 10, pp. 3571–3573, Oct. 2005.

[2] P. Vlez, I. de la Fuente, J. Bonache, and F. Martn, "Common-mode suppressed differential transmission lines based on periodic structures," in *Proc. IEEE Antennas Propag. Soc. Int. Symp.*, Jul. 2014, pp. 173–174.

[3] M. A. Varner *et al.*, "Removable EBG-based common-mode filter for high-speed signaling: Experimental validation of prototype design," *IEEE Trans. Electromagn. Compat.*, vol. 57, no. 4, pp. 672–679, Aug. 2015.

[4] S. Oh, J. Jeong, and J. Lee, "Wideband common noise suppression filter based on coupled microstrip lines and edge-coupled coplanar waveguides," *Electron. Lett.*, vol. 51, no. 25, pp. 2123–2124, 2015.

[5] M. Kim *et al.*, "Application of VSI-EBG structure to high-speed differential signals for wideband suppression of common-mode noise," *ETRI J.*, vol. 35, no. 5, pp. 827–837, 2013.

[6] A. E. Engin, "Stepped-impedance common-mode filter in differential lines," in *Proc. IEEE CPMT Symp. Jpn.*, Nov. 2016, pp. 209–212.

[7] N. P. Modi, A. Olivera, A. E. Engin, and H. Oomori, "Resonant-plane common-mode filter in differential lines," in *Proc. IEEE CPMT Symp. Jpn.*, Nov. 2017, pp. 235–238.

[8] M. Cracraft and S. Connor, "Mode-selective periodic transmission line filters to reduce radiated common-mode emissions," in *Proc. IEEE Int. Symp. Electromagn. Compat.*, Jul. 2016, pp. 216–221.

[9] D. M. Pozar, *Microwave Engineering*. New York, NY, USA: Wiley, 1998.

[10] Advanced Design System. 2016. [Online]. Available: http://www.keysight.com

[11] Sonnet v16.52. 2015. [Online]. Available: http://www.sonnetsoftware.com/

[12] A. E. Engin, W. John, G. Sommer, W. Mathis, and H. Reichl, "Modeling of striplines between a power and a ground plane," *IEEE Trans. Adv. Packag.*, vol. 29, no. 3, pp. 415–426, Aug. 2006.
[13] Ansys HFSS v13.0.[Online]. Available: http://www.ansys.com
[14] Y. Toyota, A. E. Engin, T. H. Kim, M. Swaminathan, and K. Uriu, "Stopband prediction with dispersion diagram for electromagnetic bandgap structures in printed circuit boards," in *Proc. IEEE Int. Symp. Electromagn. Compat.*, Portland, OR, USA, Aug. 2006, pp. 807–811.

Arif Ege Engin (M'05) received the B.S. degree in electrical engineering from Middle East Technical University, Ankara, Turkey, in 1998, the M.S. degree in electrical engineering from the University of Paderborn, Paderborn, Germany, in 2001, and the Ph.D. degree from the University of Hannover, Hanover, Germany, in 2004.

He worked as a Research Engineer with the Fraunhofer-Institute for Reliability and Microintegration, Berlin, Germany. From 2006 to 2008, he was an Assistant Research Director with the Microsystems Packaging Research Center, Georgia Tech. He is currently an Associate Professor with the Electrical and Computer Engineering Department, San Diego State University, San Diego, CA, USA. He has authored and coauthored more than 100 publications in journals and conferences in the areas of signal and power integrity modeling and simulation and four patents. He is the co-author of the book "*Power Integrity Modeling and Design for Semiconductors and Systems*," translated to Japanese and Chinese.

Dr. Engin was the recipient of the Semiconductor Research Corporation Inventor Recognition Award in 2009, the Outstanding Educator Award from the International Microelectronics Packaging and Assembly Society in 2015, the Alexander-von-Humboldt Research Fellowship for 2015–2018, and the 2017 IEEE EMC-S M. Kanda Award for the Most Cited Paper in the last 5 years (2013–2017).

Nisarg Modi received the B.S. degree in electronics and communication engineering from the Lalbhai Dalpatbhai College of Engineering, Ahmedabad, India, in 2014. He is currently working toward the M.S. degree in electrical and computer engineering with San Diego State University, San Diego, CA, USA.

He worked as a System Engineer with Infosys Ltd., India, from 2014 to 2016 and currently doing internship in signal integrity engineering with Intel, Santa Clara, CA. His research interests include power and signal integrity, and common-mode filter design for high-speed differential lines in printed circuit boards and package assembly.

Hiroyasu Oomori received the B.S. and M.S. degrees in electrical engineering from the Nihon University of Science and Technology, Tokyo, Japan, in 1997 and 1999, respectively.

From 1999 to 2006, he was with the Technical Research Institute, Toppan printing Co., LTD., Saitama, Japan, where he was involved in the development of the integrated circuit package and the antenna of radio-frequency identification. In 2006, he joined the Transmission Devices Laboratory, Sumitomo Electric Industries, Ltd., Yokohama, Japan, where he is involved in the development of the optical transceivers, analysis of high-speed transmission lines, and electromagnetic compatibility.